

RSC Advances



This is an *Accepted Manuscript*, which has been through the Royal Society of Chemistry peer review process and has been accepted for publication.

Accepted Manuscripts are published online shortly after acceptance, before technical editing, formatting and proof reading. Using this free service, authors can make their results available to the community, in citable form, before we publish the edited article. This *Accepted Manuscript* will be replaced by the edited, formatted and paginated article as soon as this is available.

You can find more information about *Accepted Manuscripts* in the [Information for Authors](#).

Please note that technical editing may introduce minor changes to the text and/or graphics, which may alter content. The journal's standard [Terms & Conditions](#) and the [Ethical guidelines](#) still apply. In no event shall the Royal Society of Chemistry be held responsible for any errors or omissions in this *Accepted Manuscript* or any consequences arising from the use of any information it contains.

Synthesis and Formation Mechanism of Submicrometer ZrB₂ Powders via the Pechini-Type Polymerizable Complex Route

Chunlei Yan, Rongjun Liu,* Changrui Zhang, Yingbin Cao, and Xianhai Long

Science and Technology on Advanced Ceramic Fibers and Composites Laboratory, National

University of Defense Technology, Changsha 410073, China

*Corresponding author: Rongjun Liu, Tel: +86-731-84573169, fax: +86-731-84576578, E-mail:

rongjunliu@nudt.edu.cn

Abstract ZrB₂ powders were synthesized by a polymerizable complex method based on the Pechini-type reaction route, wherein a precursor solution of citric acid, glycerol, boric acid, and zirconium ions was prepared, and polymerized to form a semitransparent resin without any precipitation at 150 °C. The precursor solutions and the resulting resins were characterized by FT-IR and ¹³C NMR spectroscopy. The results show the formation of a hybrid polymer with zirconium and boron arrested within the polymeric chain by complexation. The submicrometer ZrB₂ powders (200-600 nm) are formed after pyrolysis of the polymeric precursor with 4 B/metal molar ratios at 1400 °C. Investigation of the formation mechanism of ZrB₂ powders indicates that ZrC is the intermediary phase and two reduction reactions determine the specific pathway leading to ZrB₂ formation: (1) ZrC formation, (2) the formed ZrC directly reacts with B₂O₃ to form ZrO₂ and ZrB₂. In the whole conversion process, ZrC formation by carbothermal reduction is a fast reaction, while the direct reaction of ZrC with B₂O₃ to form ZrO₂ and ZrB₂ is the rate-limiting step.

Keywords: Zirconium diboride; Precursor; Pechini-type reaction route; Formation mechanism

Introduction

Zirconium diboride (ZrB_2) is a member of materials known as ultrahigh temperature ceramics (UHTCs). It acts as a leading role in the family of UHTCs due to its high melting point (3245 °C), high thermal conductivity ($57.9 \text{ W}\cdot\text{m}^{-1}\cdot\text{K}^{-1}$),¹ high hardness (22 GPa), good corrosion resistance, and relatively low density ($6.1 \text{ g}\cdot\text{cm}^{-3}$) and cost.² The proposed applications that take advantage of these properties include refractory linings, electrodes, cutting tools and aerospace technologies.^{1,2}

Diborides are commonly synthesized using a solid-state reaction synthesis such as boro/carbothermal reduction of corresponding oxides,³ self-propagating high-temperature synthesis (SHS)⁴ and mechanochemical synthesis.⁵ However, the ZrB_2 powder by the solid-state synthesis always suffers from a relatively coarse particle size and impurities. The liquid-based synthesis routes are expected to be effective approaches to prepare fine powders at low temperatures.⁶⁻¹² In lab, the available liquid-based synthesis routes can be divided into oxygen-free organometallic precursor route^{7,8} and oxygen-bearing sol-gel method.⁹⁻¹² The organometallic precursor route, involving forming the direct metal-boron bond, is an ideal method for metal boride synthesis. However, the need for glove box techniques, toxicity of the solvents and reagents, and high costs are key points which limit its further applications. The sol-gel method was thus extensively studied for its broad availability.⁹⁻¹² However, if less chemical interaction exists among different components, the weak intermolecular force cannot guarantee the suppression of segregation of the reaction components during so-gel transition. It is therefore crucial

to design a suitable precursor which enables the immobilization of different components in the dried gels through chemical interaction. Drawing inspiration from the Pechini method,¹³ which is based on heterometallic-citric acid complex and has been extensively used for preparation of oxide particles and films,¹⁴⁻¹⁶ an aqueous polymerizable complex route is put forward to synthesize ZrB₂ powders.

It is well known that carbothermal reduction of metal (Zr or Hf) oxides with B₂O₃ and C to form metal diborides is commonly used in the precursor system, but the reaction path taken remains ambiguous. In the beginning, Su *et al.*¹⁷ showed that transition-metal carbides of Hf and Zr were a likely reaction path to form HfB₂ and ZrB₂. Recently, Walker *et al.*¹⁸ investigated the chemical conversion process to ZrB₂ and identified ZrC as an intermediary phase route that can reduce B₂O₃ at low temperatures to form ZrB₂. On the other hand, Venugopal *et al.*¹⁹ reported that neither HfC nor B₄C was the intermediate. They further showed that the formation of HfB₂ at 1300 °C was through the intermediate formation of an amorphous B or boron suboxides, while at higher temperatures more than one reaction mechanism may be active.

In this paper, a Pechini-type polymerizable complex route based on citric acid, glycerol, zirconium oxychloride octahydrate (ZrOCl₂·8H₂O), and boric acid was used to prepare ZrB₂ precursor. We demonstrated a simple, safe, and environmentally benign method to prepare fine ZrB₂ powders at relatively low temperatures. The chemical and pyrolytic behavior of the precursor was investigated; moreover, the formation mechanism underpinning the ZrB₂ powders is also discussed to specify the

reaction path taken.

Experimental Procedure

Citric acid monohydrate, glycerol, boric acid, and zirconium oxychloride octahydrate ($\text{ZrOCl}_2 \cdot 8\text{H}_2\text{O}$) were purchased from Sinopharm Chemical Reagent Co., Ltd. and used as received. The distilled water was used as the solvents for all experiments, and no other reagents were needed.

The ZrB_2 precursor was prepared as follows. The appropriate quantities of $\text{ZrOCl}_2 \cdot 8\text{H}_2\text{O}$, citric acid, and glycerol were dissolved in distilled water under stirring at room temperature, and clear solutions were obtained over ten minutes. Afterwards, the various quantity of boric acid was added, and then the mixture was stirred at $60\text{ }^\circ\text{C}$ to form a clear solution, which was used as ZrB_2 precursor. Before the main experiments, several trial and errors were conducted to optimize the molar ratios among the $\text{ZrOCl}_2 \cdot 8\text{H}_2\text{O}$, citric acid, and glycerol. Based on these results, we set the citric acid/glycerol/zirconium molar ratio to 0.25/8/1.

All precursor solutions were placed in alumina crucibles, and then under heat treatments at $150\text{ }^\circ\text{C}$ to form dried gels. These resulting gels were yellowish semitransparent polymeric gels without any precipitation. The gels were then put into a graphite furnace which was heated in flowing argon (purity 99.999%) to the desired temperatures at $6\text{ }^\circ\text{C min}^{-1}$ and then in vacuum ($\sim 20\text{ Pa}$) at the final temperatures for 2 h. Upon cooling to room temperature, grey materials were obtained.

The Fourier transform infrared (FT-IR) spectra of the precursors were recorded on an Avatar 360 spectrometer (Nicolet) in the $4000\text{--}400\text{ cm}^{-1}$ range. Liquid-state ^{13}C

nuclear magnetic resonance (^{13}C -NMR) data was collected with a Bruker Avance-400MHz spectrometer. Solid-state ^{13}C NMR spectra were recorded on a Bruker Avance III 400 NMR spectrometer operating at 100.6 MHz using a cross-polarization magic angle spinning (CP-MAS) technique. Thermal behavior of precursor was studied by differential scanning calorimetry and thermal gravimetric analysis (DSC-TG; Netzsch STA 449F3). Powder X-ray diffraction patterns were performed on a D8 Diffractometer from Bruker instruments (Cu $K\alpha$ radiation, $\lambda=0.154$ nm). Morphology of the powder samples was observed by a scanning electron microscope (SEM; Hitachi S4800). TEM and HRTEM images were taken on a Tecnai F20 microscope operating at 200 kV.

Results and Discussion

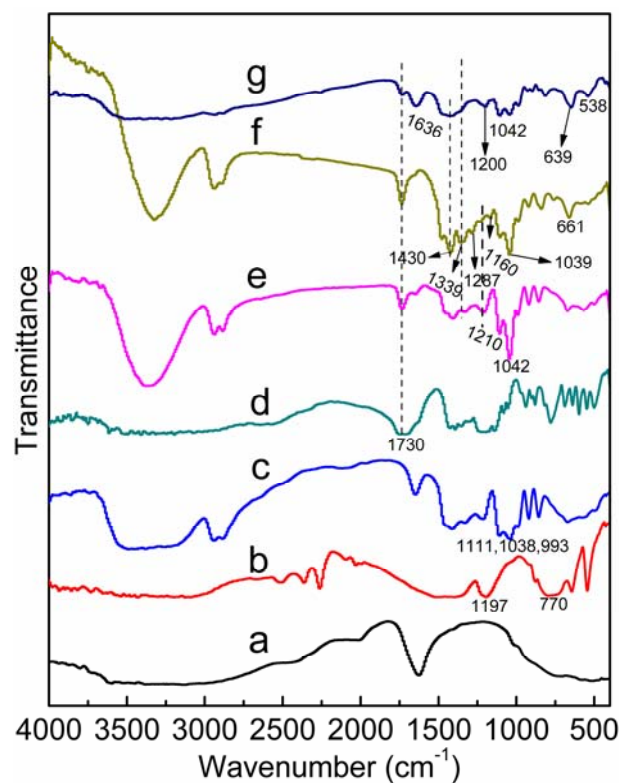


Figure 1. FT-IR spectra of (a) $\text{ZrOCl}_2 \cdot 8\text{H}_2\text{O}$, (b) boric acid, (c) glycerol, (d) citric acid, (e) bare sample of glycerol and citric acid, (f) bare sample of glycerol, citric acid

and boric acid, (g) ZrB_2 precursor. (e)-(g) were heat treated at 105 °C for 6 h.

In our ZrB_2 precursor system, the use of water as an economical and safe solvent and the easy handling of the technique contribute to the very important practical and environmentally benefits. To obtain better insight into the chemical behavior of the precursor, FT-IR and ^{13}C NMR spectra were obtained for the chemical reagents, bare samples, and ZrB_2 precursor. Figure 1 shows FTIR spectra for chemical reagents, selected bare samples, and ZrB_2 precursor. The heat treatment at 105 °C for 6 h gives viscous liquids for the selected bare samples and ZrB_2 precursor, which are all believed to be free of free water. The FT-IR spectra of $\text{ZrOCl}_2 \cdot 8\text{H}_2\text{O}$, boric acid, glycerol, and citric acid are in agreement with literature data.^{6,20} For the bare sample of glycerol and citric acid (Fig. 1e), the band at 1730 cm^{-1} due to $\nu_{\text{as}}(\text{C}=\text{O})$ becomes sharper in comparison with that of as-received citric acid, which is attributed to ester formation between glycerol and citric acid. In addition, the band at 1210 cm^{-1} for $\nu(\text{C}-\text{O})$ is the characteristic band of ester group, further confirming the occurrence of esterification reaction. The esterification reaction also changes the relative intensity of the three bands at $\sim 1042 \text{ cm}^{-1}$ for $\nu(\text{C}-\text{O})$ of the glycerol. After the introduction of boric acid, the glycerol has a tendency to form borate ester with boric acid, thus FTIR spectrum (Fig. 1f) presents many differences. The new peaks at 1287 cm^{-1} and 1160 cm^{-1} are corroborated to characteristic stretching vibrations of B-O-C bonds,^{20,21} providing strong evidence for the reaction between glycerol and boric acid to form borate ester. Besides, the absorption bands at 1430, 1339 cm^{-1} are assigned to stretching vibration and bending mode of B-O, respectively.^{22,23} Furthermore, the

B-O-H bending band at 1197 cm^{-1} and O-H torsion band at 770 cm^{-1} derived from boric acid disappear in the condensed products,²¹ and the intensity of the bands at $\sim 1039\text{ cm}^{-1}$ for $\nu(\text{C-O})$ of the glycerol get weaker accordingly. All these results further confirm the esterification reaction between glycerol and boric acid. As discussed elsewhere,⁹ the esterification reaction leads to formation of hexatomic or pentatomic ring of B-glycerol chelating complex with remaining free alcoholic hydroxyl group. These remaining hydroxyl groups can further react with citric acid to form a rigid polymer through esterification reaction. After introduction of zirconium ion to form the ZrB_2 precursor, its FTIR spectrum (Fig. 1g) exhibits some changes in addition to the similar bands related to the vibration of B-O bond. The striking result is that the presence of zirconium ions split the band at 1730 cm^{-1} for zirconium-free sample into two bands located at 1730 and 1636 cm^{-1} for the ZrB_2 precursor. Especially for the latter at 1636 cm^{-1} , it appears nearly 100 cm^{-1} lower than zirconium-free samples, which confirms the coordination of citric acid to the zirconium ion.²⁴ Meanwhile, the bands at 639 and 538 cm^{-1} due to the vibrations of Zr-O further confirm the coordination of citric acid to metal ion. Moreover, the band at 1200 cm^{-1} due to $\nu(\text{C-O})$ of the ester group and the changes of bands at 1042 cm^{-1} assigned to $\nu(\text{C-O})$ of the glycerol indicate the esterification reaction between citric acid-zirconium complex and glycerol to form the polymer.

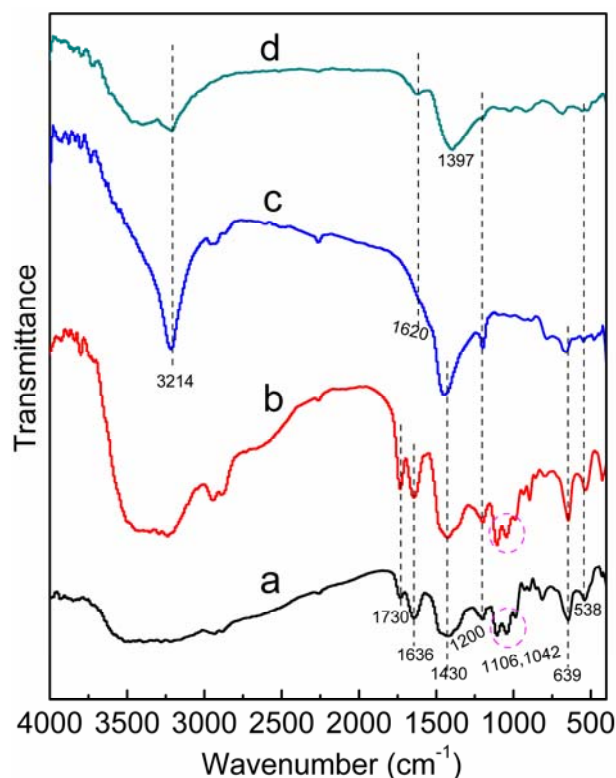


Figure 2. FT-IR spectra of ZrB_2 precursor after heat treatment at (a) 105, (b) 150, (c) 250, (d) 350 °C for 6 h. The heat treatments of 250 and 350 °C are under argon atmosphere, while the rest are in air.

FT-IR spectra of ZrB_2 precursor heat-treated at selected temperatures are shown in Fig. 2. Spectrum of ZrB_2 precursor dried at 150 °C shows similar infrared bands to that dried at 105 °C. The band at 1636 cm^{-1} due to the $\nu_{as}(C=O)$ of the carboxylate group and the bands at 639, 538 cm^{-1} for Zr–O get stronger, indicating the high stability of the coordinated structure. Besides, the stronger bands at 1430 cm^{-1} for B–O bond and 1200 cm^{-1} for $\nu(C-O)$ of ester group indicates that the higher temperature promotes the esterification reaction to form the polymer gels. When the precursor is heated up to 250 °C, significant differences appear for FT-IR spectrum compared to that dried at 150 °C, indicating great changes in the molecular structure. Specifically, the bands at 1730 and 1636 cm^{-1} due to $\nu_{as}(C=O)$ of the carboxylate

groups almost disappear and the bands at 639, 538 cm^{-1} for Zr–O get weaker. Moreover, the bands at 1042, 1106 cm^{-1} due to $\nu(\text{C-O})$ of the glycerol disappear, while the band at 1200 cm^{-1} for $\nu(\text{C-O})$ of the ester group remains. The absorption band at 1430 cm^{-1} assigned to stretching vibration of B–O exhibits stronger, indicating the further formation of borate ester. The sharp band at 3214 cm^{-1} due to $\nu(\text{O-H})$ is believed to be originated from the remaining carboxylate groups. The weak shoulder band located at $\sim 1620 \text{ cm}^{-1}$ indicates the occurrence of the alkenes, and this is further confirmed by the spectrum at 350 $^{\circ}\text{C}$. In addition to the band due to alkene, the changes of $\nu(\text{O-H})$, $\nu_{\text{as}}(\text{C=O})$, $\nu(\text{C-O})$ and $\nu(\text{Zr-O})$ suggest that the dehydroxylation and decarboxylation take place, indicating the occurrence of in-situ carbonization.

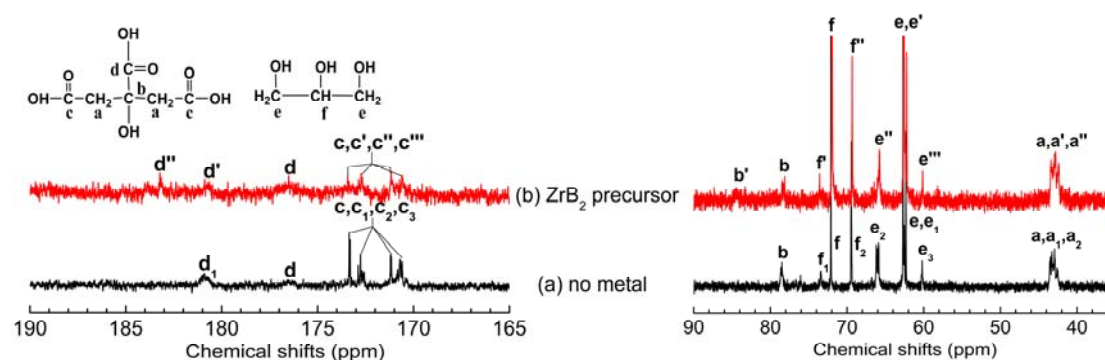


Figure 3. Liquid-state ^{13}C NMR spectra of (a) bare sample only without zirconium addition and (b) ZrB_2 precursor.

Figure 3 shows the liquid-state ^{13}C NMR spectra of bare sample only without zirconium addition and ZrB_2 precursor solutions using D_2O as a solvent. These samples were prepared by dissolving the reagents in D_2O in a few minutes and were subjected to liquid-state ^{13}C NMR test immediately. For the sake of convenience, the symbols on the peak show assignments of NMR peaks to carbon centers of the molecule (inset in Fig. 3) and their derivatives. The ^{13}C NMR spectrum for bare

sample without metal addition is shown in Fig. 3a. Despite the limited reaction time, some extra peaks (a_1 , a_2 , c_1 , c_2 , c_3 , e_1 , e_2 etc. as defined in Fig. 3a) assigned to carbon centers of esterified derivatives are observed in addition to the signals (a, b, c, d, e, f) due to the as-received glycerol and citric acid.^{24,25} It should be noted that the esterified derivatives may also originate from esterification reaction of boric acid with alcoholic hydroxyl and carboxylate groups (the esterification reaction between carboxylate group and boric acid was also discussed elsewhere²¹). It is noteworthy that more derivative peaks from the terminal carboxyl groups than the central carboxyl group appear, indicating the preferential reaction of the terminal carboxyl. After the introduction of zirconium ion to form the ZrB_2 precursor, its ^{13}C NMR spectrum exhibits some differences. The signals (e, e', e'', e''', f, f', f'') due to glycerol and its derivatives show no shifts and similar strength to that of bare sample, indicating that little complexation occurs between zirconium ion and glycerol. However, the ^{13}C NMR results do confirm the complexation of citric acid to zirconium ion. First, the striking result is that the presence of zirconium ions weakens the signals due to the carbon from carboxyl groups, which is attributed to coordination of the carboxyl groups to zirconium ion. Moreover, a new peak assigned to the central carboxyl group appears at 183.2 ppm, which shifts to lower field region when it coordinates with the zirconium ion. Second, in the higher field region, noteworthy are the signals due to alcoholic carbon (carbon b) of citric acid. In addition to the weak resonance at 78.5 ppm similar to the bare sample, the ZrB_2 precursor gives rise to a new resonance at 84.5 ppm associated with the alcoholic carbon (carbon b). As

discussed elsewhere,^{24,25} this new resonance can be assigned to the central carbon in citric acid with dissociation of the proton from the hydroxy group which bonds to the same carbon. Thus, the deprotonated alkoxide oxygen atom is likely to bridge the zirconium ions, together with two terminal carboxylic acid groups to build fused six-membered chelate rings. It can be observed that the presence of zirconium ion does not affect the esterification reaction, as the derivative signals from both citric acid and glycerol still appear in ^{13}C NMR of ZrB_2 precursor. Thus, in combination with the FT-IR results, it can be concluded that the polymerization between citric acid and glycerol gives rise to a polymer chain with sites available to form chelates with Zr ion and boric acid, so as to inhibit the segregation of components throughout the resulting gel.

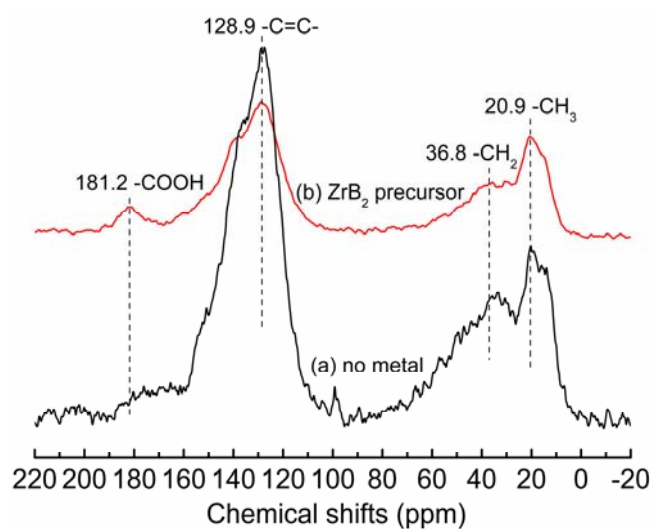


Figure 4. Solid-state ^{13}C NMR spectra of (a) bare sample only without zirconium addition and (b) ZrB_2 precursor dried at 250 °C for 6 h.

Solid-state ^{13}C NMR spectra of bare sample and ZrB_2 precursor dried at 250 °C are shown in Fig. 4. The ^{13}C NMR spectrum of ZrB_2 precursor dried at 250 °C is similar to that of the bare sample. Three strong peaks appear at ~20.9, ~36.8, and ~128.9 ppm

for both bare sample and ZrB_2 precursor, which are attributed to CH_3 , $-CH_2-$ and unsaturated carbon ($C=C$), respectively.²⁴ The remaining CH_3 , $-CH_2-$ and unsaturated carbon ($C=C$) groups indicate the occurrence of carbonization as the decarboxylation and dehydration are proceeding. Note that the resonance at 181.2 ppm (Fig. 4b) due to carbons centers of carboxylate groups for ZrB_2 precursor still retains, while the corresponding resonance for the bare sample is weak and not distinct, indicating that the existence of complex inhibits the decarboxylation of citric acid. The coexistence of the complexation and carbonization shows the tendency to achieve intimate mixing of the components during the pyrolysis of the precursor.

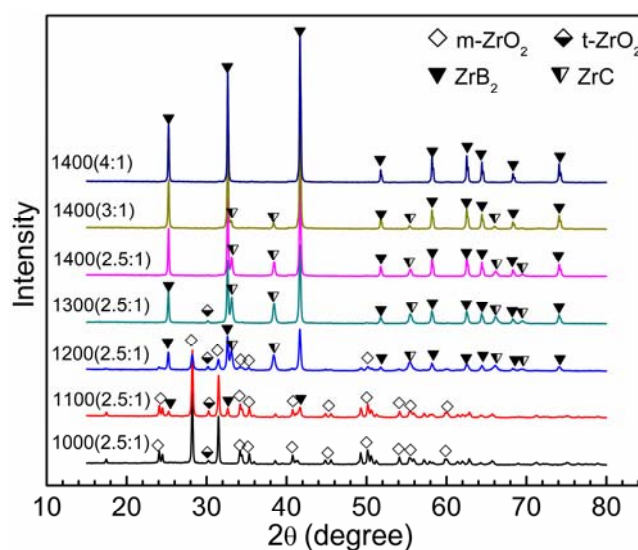


Figure 5. XRD patterns of ZrB_2 precursors with various B/metal molar ratios (in brackets) pyrolysed at varying temperatures ($^{\circ}C$).

In the following heat treatments leading to boride formation, the thermal behavior, the phase and morphology evolution, conversion mechanism of the precursor were studied by XRD, TG-DSC, SEM, and TEM techniques. Figure 5 shows XRD patterns of ZrB_2 precursors with various B/metal molar ratios pyrolysed at varying

temperatures. XRD pattern of 1000 °C shows only ZrO_2 without ZrB_2 formation, and the initial formation of ZrB_2 can be observed at 1100 °C. At 1200 °C, ZrB_2 has become the major phase despite a considerable amount of ZrO_2 phase; moreover, noteworthy is the new ZrC phase, which is not observed at 1100 °C. After heat treatments at 1300 °C, the precursor has been almost transformed into non-oxidic phase with a little t-ZrO_2 phase as a remnant, however, in addition to the major ZrB_2 phase, the minor ZrC phase can also be observed. In the following heat treatments of 1400 °C, a non-oxidic material is obtained for the ZrB_2 precursors with 2.5 B/metal molar ratios; besides, the ZrC phase has been partially transformed into ZrB_2 . The remaining ZrC phase suggests the insufficiency of boron source; therefore, different B/metal molar ratios are used to study their effects on the transformation of the ZrB_2 precursors at 1400 °C. The XRD patterns show that with the increase of B/metal molar ratio, the amount of ZrC decreases, and the ZrC has been completely transformed into ZrB_2 for 4 B/metal molar ratio. It is well known that B_2O_3 has a high vapor pressure at high temperatures, so the excessive B_2O_3 is necessary to complete carbothermal reduction reaction to form the stoichiometric ZrB_2 .

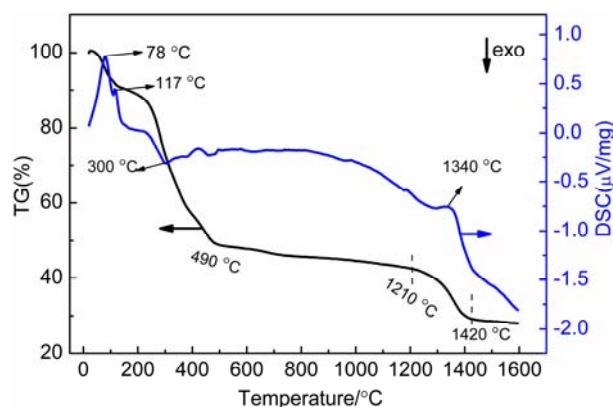


Figure 6. TG-DSC curves for ZrB_2 precursor powder.

The thermal behavior of ZrB_2 precursor was studied by DSC-TG analysis as shown in Fig. 6. The TG curve indicates three rapid weight loss regions, i.e. 80-150, 220-490 and 1210-1420 °C. The weight loss in the region of 80-150 °C is due to the evaporation of water, including physisorbed water and the water originating from the intermolecular dehydration via esterification reaction, which results in endothermic peaks at 78 °C and 117 °C in the DSC curve, respectively. The weight loss at 220-490 °C is observed as the dehydration, polymerization, and finally the carbonization are proceeding in this temperature region, which leads to a wide exothermic peak at ~300 °C. The high temperature weight loss at 1210-1420 °C is believed to be attributed to the carbothermal reduction reaction; moreover, the DSC curve shows endothermic heat flow at 1340 °C, indicating the beginning of the reduction process.

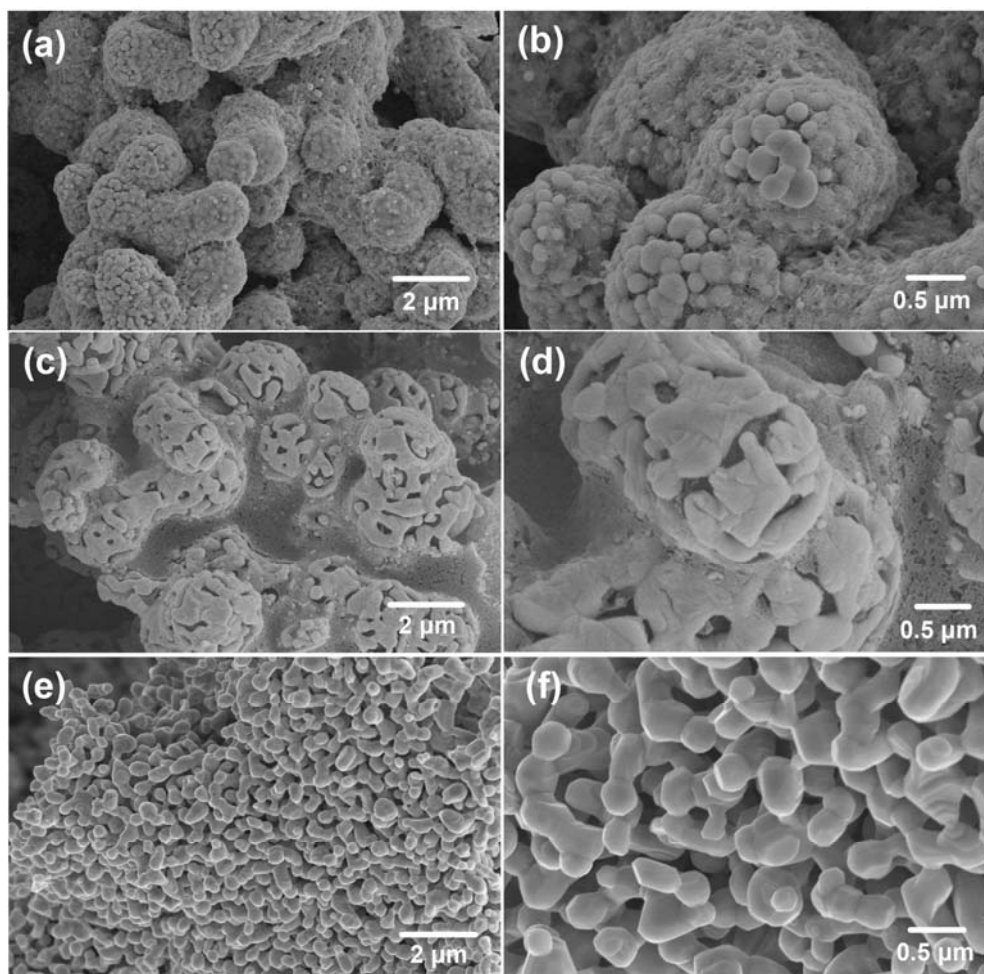


Figure 7. SEM images of ZrB_2 precursor heat-treated at (a-b) 1000, (c-d) 1200, (e-f) 1400 °C.

Morphology evolution of ZrB_2 precursor heat treated at various temperatures is shown in Fig. 7. Figure 7a-b reveals the typical morphology of ceramic product at 1000 °C. The product is comprised of many large sphere-like lumps in disorder piles. On closer observation of the sphere-like lumps, they consist of small crystal particles “glued” together by flocculus materials. The widely distributed flocculus materials are believed to be the mixture of amorphous carbon and glassy B_2O_3 , which will be consumed by the following carbothermal reduction reactions. Further increase in pyrolysing temperature to 1200 °C leads to some differences in the morphology

compared with that at 1000 °C. Firstly, the flocculus materials are consumed significantly, especially for the top areas of the sphere-like lumps. This result confirms the speculation that the flocculus materials are the mixture of amorphous carbon and glassy B₂O₃, which are consumed by the intensive transformation of ZrO₂ to ZrB₂ at 1200 °C. Secondly, after consumption of flocculus materials, a new coral-like product without clear crystal form appears at the top areas of lumps and is expected to be the ZrB₂ according to the XRD results. Figure 7e-f shows that the flocculus materials are completely consumed for ZrB₂ precursor (4 B/metal molar ratios) heat treated at 1400 °C. The final ZrB₂ powders consist of well-defined, nearly spherical crystal particles. It can be roughly estimated from the magnified image shown in Fig. 7f that the particle size lies in the range of 200–600 nm.

As discussed in the introduction section, the major disputes about the formation mechanism are focused on the intermediary phase that leads to formation of diborides. Based on the given results, the reaction path can be divided into two categories, i.e. one involves the intermediary phase of carbides,^{17,18} while another concerns the intermediary phase of amorphous B or boron suboxides.¹⁹ To clarify the specific reaction path taken still awaits more details to be unveiled. Herein, transmission electron microscopy (TEM, Fig. 8) was used to investigate the microstructural development of ZrB₂ precursor. Furthermore, two bare samples (one contains the boric acid, citric acid and glycerol, another consists of zirconium, citric acid and glycerol) were prepared to clarify the possible intermediary phase formed (Figs. 9 and 10).

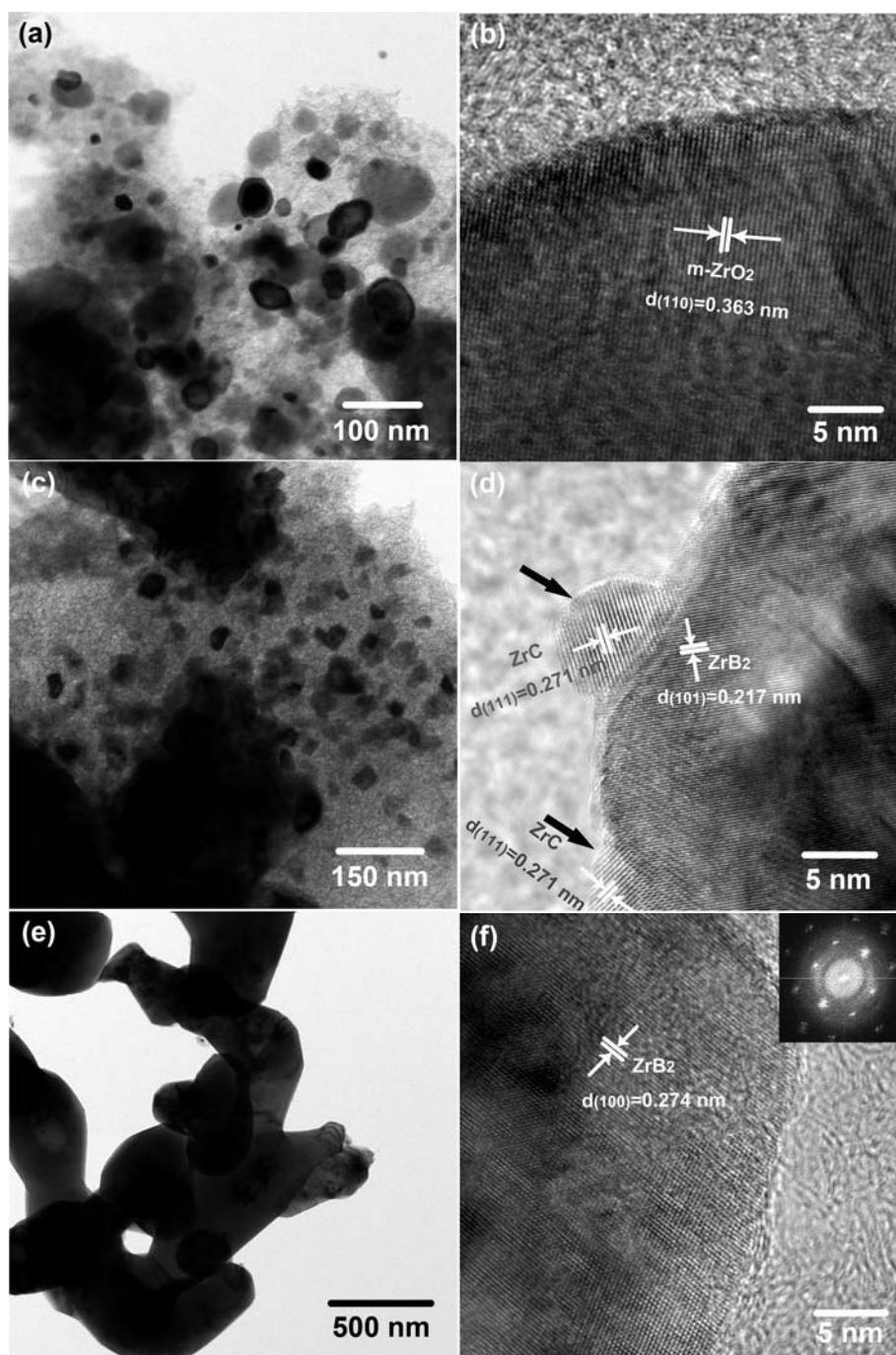


Figure 8. (a, c, e) TEM and (b, d, f) HRTEM images of ZrB_2 precursor heat-treated at (a-b) 1000, (c-d) 1200, (e-f) 1400 °C, the inset is the corresponding fast Fourier transform (FFT) of the image.

Figure 8 shows TEM images of ZrB_2 precursor heat-treated at various temperatures. The TEM image of products at 1000 °C (Fig. 8a) shows that many small particles are homogeneously distributed in a flocculus matrix. According to the XRD and SEM

results, the small particles and flocculus matrix are believed to be ZrO_2 and mixture of carbon and B_2O_3 , respectively. The products at 1000 °C can be thus well described as $\text{ZrO}_2/\text{carbon}/\text{B}_2\text{O}_3$ nanocomposites, which consist of ZrO_2 crystallites, about 50 nm in size, highly distributed within a matrix of carbon and B_2O_3 . Therefore, the objective to obtain the ZrO_2 , carbon, and B_2O_3 intimately mixed has been achieved by the polymerizable complex route. These intimately mixed components promote reaction kinetics for shortening the diffusion distances, hence lower reaction temperatures with corresponding benefits in the final product size. High-resolution transmission electron microscopy (HRTEM, Fig. 8b) of a single particle indicates that the well-crystallized ZrO_2 is surrounded by amorphous materials. The lattice spacing is 0.363 nm, in good agreement with the known value for (110) planes of m- ZrO_2 (ICDD-PDF #65-1025). When the ZrB_2 precursor is heat-treated at 1200 °C, XRD results show that the intensive transformation of ZrO_2 to ZrB_2 takes place, nevertheless, the minor phases including ZrO_2 and ZrC can also be observed in addition to the major ZrB_2 phase. The TEM picture at 1200 °C (Fig. 8c) shows both the heavily aggregated particles and dispersed small particles in amorphous matrix. These dispersed particles have a similar size of ~50 nm to that at 1000 °C without visible particle size growth, whose size is also consistent with the average size of 43 nm estimated by the Sherrer formula. A closer inspection of a single representative particle (Fig. 8d) by HRTEM reveals further microstructural details on the formation of ZrB_2 powders. The main body of the particle shows well crystalline state and shares interplanar spacing of 0.217 nm, which is consistent with the known value for (101) lattice fringe of ZrB_2 (ICDD-PDF

#34-0423), giving strong evidence that this particle is ZrB₂. Noteworthy are the edge parts of this particle (the arrows denotes in Fig. 8d), which are “attached” to the main body and exhibit a small size. Moreover, a lattice spacing of $d_{(111)}=0.271$ nm is observed for these parts and is consistent with the known value for ZrC (ICDD-PDF #65-4932), giving convincing evidence that they are ZrC. On closer observation of the contacting areas of the two parts to the main ZrB₂ body, the “front line” of the ZrB₂ crystallite is encroaching towards the ZrC areas, in other words, these ZrC parts are gradually fused into the main ZrB₂ body. It can be thus concluded that the in-situ transformation of ZrC to ZrB₂ crystallite is recorded, which gives strong evidence that ZrC is the intermediary phase leading to ZrB₂ formation. After heat treatments at 1400 °C, the ZrB₂ precursor with 4 B/metal molar ratios has been completely transformed into ZrB₂ according to the XRD results. Its TEM image (Fig. 8e) shows that amorphous materials at 1200 °C completely disappear, and well-defined and weakly aggregated ZrB₂ powders are obtained. The final ZrB₂ powders produced by our precursor route have a particle size ranging from 200 to 600 nm by TEM image (Fig. 8e), which show significant particle growth compared with powders at 1200 °C. Here in this case, it is believed that the Ostwald ripening dominates the particle growth at the expense of the small intermediate particles. The HRTEM image of ZrB₂ particle is shown in Fig. 8f. This well-crystallized particle possesses an interplanar distance of 0.274 nm, corresponding well to the $d_{(100)}$ plane of ZrB₂ bulk. Moreover, the inset FFT of the same particle proves the single crystallinity of the particle.

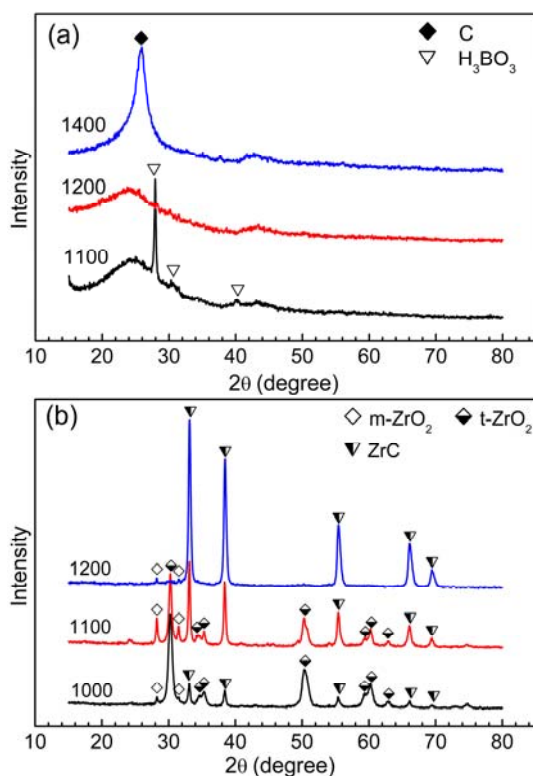
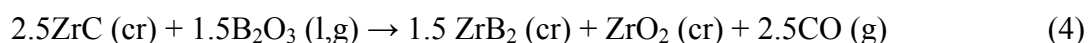
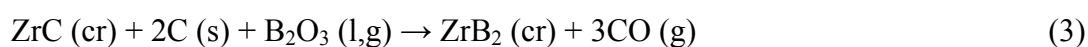
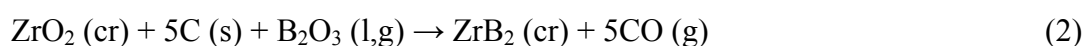
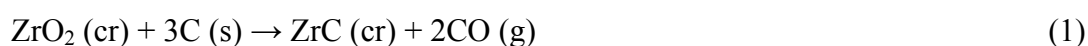


Figure 9. XRD patterns of bare samples pyrolysed at varying temperatures ($^{\circ}\text{C}$): (a) sample consisting of boric acid, citric acid and glycerol without zirconium addition, (b) sample containing zirconium, citric acid and glycerol without boric acid addition.

In order to shed further light on the intermediary phase formed during the transformation of ZrB_2 precursor, two bare samples were prepared and their XRD patterns at varying temperatures are shown in Fig. 9. One potential intermediate phase route is based on B_2O_3 reduction by carbon to form the B or B_4C or boron suboxides. If this is the case then these B-containing intermediate phases have to form below $1100\text{ }^{\circ}\text{C}$, i.e., at a temperature lower than that required for ZrB_2 formation. Figure 9a shows the XRD patterns of sample consisting of boric acid, citric acid and glycerol without zirconium addition. At $1100\text{ }^{\circ}\text{C}$, the only crystalline phase formed is H_3BO_3 , which is attributed to the water sorption of the remaining B_2O_3 . With increase in pyrolysing temperature to $1200\text{ }^{\circ}\text{C}$, in addition to the humps at 25 degrees due to

pyrolysed carbon, no crystalline phases are detected. No crystalline B-containing phases can be observed yet, even if the pyrolysing temperature increases to 1400 °C. Neither B and boron suboxides nor B₄C is detected even up to 1400 °C, which suggests that it is an unlikely route for low-temperature synthesis of ZrB₂. On the other hand, the carbothermal reduction of ZrO₂ (reaction (1)) in bare sample without boric acid addition has been observed to start taking place at as low as 1000 °C, which is lower than 1100 °C required for ZrB₂ formation. After heat treatments at 1100 °C, the bare sample has been intensively transformed into ZrC (major phase of the products), where ZrB₂ starts to form. With further increase of temperature to 1200 °C, the bare sample has been almost completely transformed into ZrC, where ZrB₂ become the major phase for ZrB₂ precursor. Therefore, in combination with the results of in-situ transformation of ZrC to ZrB₂ by TEM, it can be confirmed that ZrC is the intermediary phase leading to ZrB₂ formation.



The overall oxide-based starting chemistry reaction to form ZrB₂ by a single carbothermal reduction step is shown in reaction (2). However, the specific pathways considering the ZrC as the intermediary phase leading to ZrB₂ formation still remain ambiguous. There are two pathways reported by which ZrC can react to form ZrB₂. Su et al.¹⁷ reported the initial formation of carbides and boron oxide is followed by a

fast reaction to produce the borides shown as reaction (3). Luke et al.¹⁸ developed this pathway by combining the reactions (3) and (4). They reported that at low temperatures ($\sim 1200^\circ\text{C}$), ZrC formation is limiting, and ZrC is found to be a direct reducing agent for B_2O_3 to form ZrB_2 and ZrO_2 , whereas at high temperatures ($\sim 1500^\circ\text{C}$) the reaction of ZrC to ZrB_2 becomes rate limiting, and it reacts with B_2O_3 and C to form pure ZrB_2 . Here lies the problem that it is the reactions (3) and (4) or the overall reaction (3) or other mechanism to determine the formation mechanism of ZrB_2 . Based on the above mentioned pathway, herein, a specific pathway consisting of two reduction reactions (1) and (4) is more reasonable to explain the formation mechanism. In light of reactions (1) and (4), the overall oxide-based reaction (2) can be obtained by eliminating ZrC item of reactions (1) and (4), whereas the overall carbide-based reaction (3) can be obtained by eliminating ZrO_2 item. Therefore, it is the two reduction reactions (1) and (4) that determine the specific pathway leading to ZrB_2 formation. Nevertheless, which reaction is the limiting step is needed to be further discussed. In our case, the bare sample forms ZrC at 1000°C and has been almost completely transformed into ZrC at 1200°C ; hence ZrC formation (reaction (1)) is a fast reaction and should not be the limiting step. Thus the direct reaction of ZrC with B_2O_3 to form ZrB_2 and ZrO_2 (reaction (4)) is believed to be the rate limiting step.

If reaction (4) is the rate limiting step, the intermediary ZrC always remains in the products. However, the initial formation of ZrB_2 without any ZrC intermediate can be observed at 1100°C . The answer lies in ZrC itself. At 1100°C , the ZrC has become

the major phase in the bare sample and its TEM images are shown in Fig. 10. The particles exhibit a size of 20-50 nm, and a closer inspection of a single particle reveals that many nanocrystalline inclusions (the dashed circles in Fig. 10b) are observed. These inclusions share the lattice spacing of $d_{(111)} \approx 0.270$ nm, in good agreement with the known value for ZrC, besides; It is notable that these inclusions have different orientations and parts of them involve dislocations. The fine surface areas and defects of the particles will contribute to their high reactivity, potentially reducing reaction temperatures. Moreover, B_2O_3 is much excessive in relative to the formed ZrC, so intermediary phase ZrC has been completely transformed into ZrB_2 at 1100 °C. With increase of temperature, B_2O_3 volatilizes fast due to its high vapor pressure, thus intermediary phase ZrC remains in the precursor heated at 1200-1400 °C with 2.5 B/metal molar ratios. Hence reaction (4) starts to perform as a visible rate limiting step. However, at 1300 and 1400 °C, we cannot observe almost any ZrO_2 but ZrB_2 and ZrC as the formed ZrO_2 by reaction (4) immediately reacts to form ZrC via the fast reaction (1). Finally, the ZrC has been completely transformed into ZrB_2 when the B/metal molar ratio increases to 4. It can be thus concluded that in the whole conversion process, ZrC formation by carbothermal reduction (reaction (1)) is a fast reaction, while the direct reaction of ZrC with B_2O_3 (reaction (4)) to form ZrO_2 and ZrB_2 is the rate limiting step.

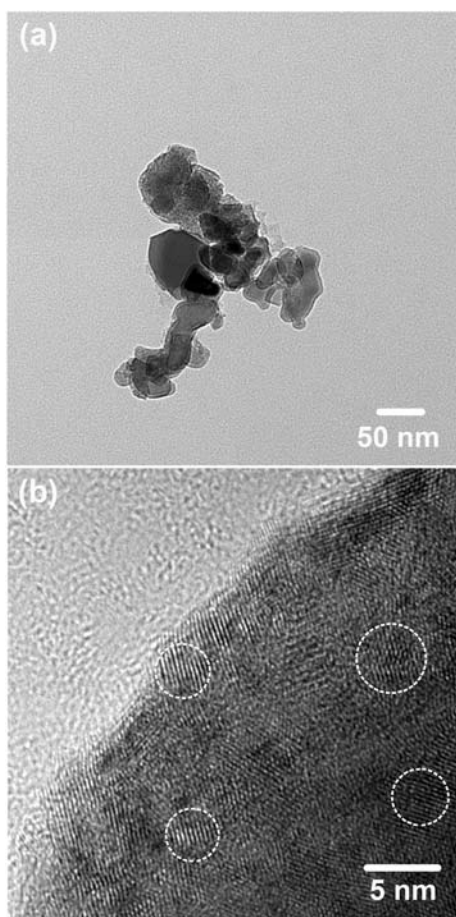


Figure 10. TEM images of bare sample consisting of zirconium, citric acid and glycerol heat-treated at 1100 °C.

Conclusions

ZrB₂ powders were successfully synthesized by a Pechini-type polymerizable complex route. Heating of a precursor solution of citric acid, glycerol, boric acid, and zirconium ions at 150 °C produced a semitransparent resin without any precipitation. The polymerization between citric acid and glycerol gave rise to a polymer chain with sites available to form chelates with the Zr ion and boric acid, so as to immobilize zirconium and boron within this polymeric chain. Pyrolysis of this polymeric precursor with 4 B/metal molar ratios produced high-purity submicrometer ZrB₂ powders (200-600 nm) at 1400 °C. Investigation of the formation mechanism of ZrB₂

indicates that ZrC is the intermediary phase and the specific pathway leading to ZrB₂ formation involved two reduction reactions: (1) ZrC formation, (2) the formed ZrC directly reacts with B₂O₃ to form ZrO₂ and ZrB₂. In the whole conversion process, ZrC formation by carbothermal reduction is a fast reaction, while the direct reaction of ZrC with B₂O₃ to form ZrO₂ and ZrB₂ is the rate-limiting step. Specifically, at low temperature (1100 °C), the formed ZrC has been completely transformed into ZrB₂ for the high reactivity of ZrC and excess of B₂O₃. However, further increase in temperature leads to evaporation of B₂O₃, as a result, the ZrC cannot be completely transformed into ZrB₂ even at 1400 °C unless the 4 B/metal molar ratios were used.

Acknowledgements

This work was financially supported by the National Natural Science Foundation of China (no. 51102282) and Aid Program for Science and Technology Innovative Research Team in Higher Educational Institutions of Hunan Province.

References

- 1 J. K. Sonber and A. K. Suri, *Adv. Appl. Ceram.*, 2011, **110**, 321.
- 2 W. G. Fahrenholtz and G. E. Hilmas, *J. Am. Ceram. Soc.*, 2007, **90**, 1347.
- 3 C. Mroz, *Am. Ceram. Soc. Bull.*, 1994, **73**, 141.
- 4 D. D. Radev and D. Klissurski, *J. Mater. Synth. Process.*, 2001, **9**, 131.
- 5 N. Setoudeh and N. J. Welham, *J. Alloys Compd.*, 2006, **420**, 225.
- 6 C. L. Yan, R. J. Liu, C. R. Zhang and Y. B. Cao, *RSC Adv.*, 2015, **5**, 36520.
- 7 Z. F. Xie, T. Zhou and Y. Z. Gou, *Ceram. Int.*, 2015, **41**, 6226.
- 8 J. Yuan, S. Hapis, H. Breitzke, Y. Xu, C. Fasel, H. Kleebe, G. Buntkowsky, R.

- Riedel and E. Ionescu, *Inorg. Chem.*, 2014, **53**, 10443.
- 9 G. Ji, H. Ji, M. Li, X. Li and X. Sun, *J. Sol-Gel Sci. Technol.*, 2014, **69**, 114.
- 10 G. Cheng, *Int. J. Refract. Met. Hard Mater.*, 2013, **36**, 149.
- 11 R. Li, Y. Zhang, H. Lou, J. Li and Z. Feng, *J. Sol-Gel Sci. Technol.*, 2011, **58**, 580.
- 12 Y. Xie, T. H. Sanders Jr. and R. F. Speyer, *J. Am. Ceram. Soc.*, 2008, **91**, 1469.
- 13 M. Pechini and N. Adams, US Pat., 3 330 697, 1967.
- 14 D. Segal, *J. Mater. Chem.*, 1997, **7**, 1297.
- 15 S. G. Rudisill, N. M. Hein, D. Terzic and A. Stein, *Chem. Mater.*, 2013, **25**, 745.
- 16 M. S. J. Nunes, E. R. Leite, F. M. Pontes, N. M. Duboc, E. Longo and J. A. Varela, *Mater. Lett.*, 2001, **49**, 365.
- 17 K. Su and L. G. Sneddon, *Chem. Mater.*, 1993, **5**, 1659.
- 18 L. S. Walker and E. L. Corral, *J. Am. Ceram. Soc.*, 2014, **97**, 399.
- 19 S. Venugopal, E. E. Boakye, A. Paul, K. Keller, P. Mogilevsky, B. Vaidhyanathan, J. G. P. Binner, A. Katz and P. M. Brown, *J. Am. Ceram. Soc.*, 2014, **97**, 92.
- 20 I. Yanase, R. Ogawara and H. Kobayashi, *Mater. Lett.*, 2009, **63**, 91.
- 21 R. Dina, G. H. Zahida, Z. Asghara, M. Maqbool, E. Ahmad and T. Azhar, *J. Asian Ceram. Soc.*, 2014, **2**, 268.
- 22 O. Koysuren, M. Karaman and H. Dinc, *J. Appl. Polym. Sci.*, 2012, **124**, 2736.
- 23 H. Aydin and A. Bozkurt, *J. Mater. Res.*, 2014, **29**, 625.
- 24 J. Tsay and T. Fang, *J. Am. Ceram. Soc.*, 1999, **82**, 1409.
- 25 M. Kakihana, M. Arima, Y. Nakamura, M. Yashima and M. Yoshimura, *Chem. Mater.*, 1999, **11**, 438.